

THE OFFICIAL MAGAZINE OF THE OCEANOGRAPHY SOCIETY

Oceanography

CITATION

Dohan, K., H.-Y. Kao, and G.S.E. Lagerloef. 2015. The freshwater balance over the North Atlantic SPURS domain from Aquarius satellite salinity, OSCAR satellite surface currents, and some simplified approaches. *Oceanography* 28(1):86–95, <http://dx.doi.org/10.5670/oceanog.2015.07>.

DOI

<http://dx.doi.org/10.5670/oceanog.2015.07>

COPYRIGHT

This article has been published in *Oceanography*, Volume 28, Number 1, a quarterly journal of The Oceanography Society. Copyright 2015 by The Oceanography Society. All rights reserved.

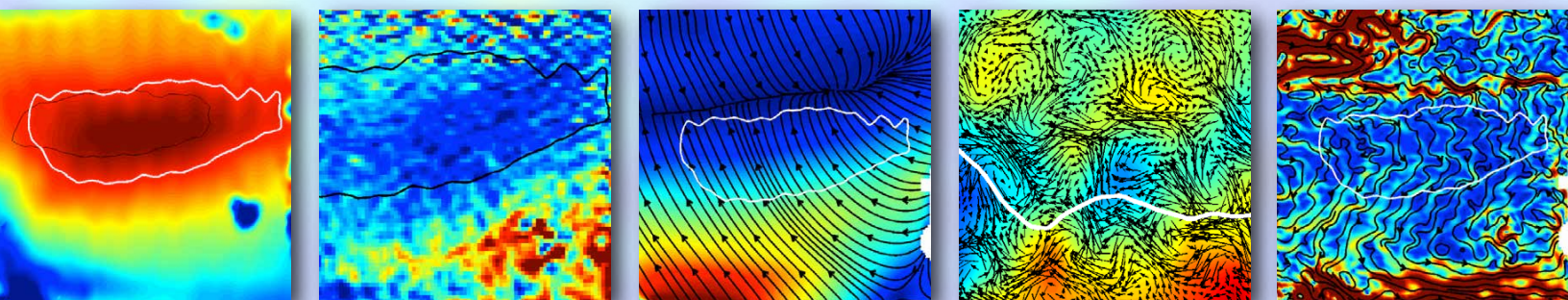
USAGE

Permission is granted to copy this article for use in teaching and research. Republication, systematic reproduction, or collective redistribution of any portion of this article by photocopy machine, reposting, or other means is permitted only with the approval of The Oceanography Society. Send all correspondence to: info@tos.org or The Oceanography Society, PO Box 1931, Rockville, MD 20849-1931, USA.

The Freshwater Balance

Over the North Atlantic SPURS Domain from Aquarius Satellite Salinity,
OSCAR Satellite Surface Currents, and Some Simplified Approaches

By Kathleen Dohan, Hsun-Ying Kao, and Gary S.E. Lagerloef



ABSTRACT. Within the North Atlantic subtropical gyre lies a salinity maximum region, relatively constant in time, yet forced by a seasonally varying strong evaporation zone located several degrees south and advected by wind-driven Ekman currents and geostrophic gyre currents and eddies. Large-scale calculations using in situ salinities to quantify salt divergence in the mixed layer, together with freshwater flux products, cannot account for the observed surface salinity signature. Small-scale and vertical processes must complete the budget. The Aquarius satellite system, launched in June 2011, now provides sea surface salinity observations every seven days at approximately 100 km spacing. Here, we reexamine the surface freshwater balance in the salinity maximum region, the location of the Salinity Processes in the Upper-ocean Regional Study (SPURS) campaign, from a satellite-sensed perspective. Advection of surface salinity by Ocean Surface Current Analyses Real-time (OSCAR) satellite-based surface currents is investigated for the whole region as well as within two boxes that isolate the salinity maximum and the maximum evaporation regions. Locations of imbalance, variability of surface salinity forcing terms, and areas of potential transport and redistribution are explored using satellite observations. A discussion then considers the vertical pathways by which surface waters reach and exchange salinity with the deep ocean, thus contributing to the signal seen at the surface.

THE SALINITY MAXIMUM REGION IN THE NORTH ATLANTIC SUBTROPICAL GYRE

Regions of maximum salinity occur roughly in the center of all subtropical gyres, and the strongest of them is centered near 25°N, 325°E in the North Atlantic. This region is stable, with almost no change in surface salinity with time compared to surrounding areas. This North Atlantic subtropical salinity maximum was the focus of the initial Salinity Processes in the Upper-ocean Regional Study (SPURS-1) field campaign designed to improve understanding of the mechanisms that maintain the regional high surface salinities and understanding of the surface freshwater flux budget.

In June 2011, prior to the start of the campaign, the US National Aeronautics and Space Administration (NASA) in partnership with Argentina's space agency, Comisión Nacional de Actividades Espaciales (CONAE), launched a new Aquarius/SAC-D satellite system (Lagerloef et al., 2012; Lagerloef, 2014) that can measure sea surface salinity (SSS). A key science objective of the satellite salinity mission is to significantly improve understanding of net air-sea freshwater flux. Salinity variability is a useful indicator of changes in the global hydrological cycle over the ocean. By analyzing upper-ocean salinity, we are able to examine vertical mixing rates, the distribution of the water masses in the ocean, and eventually the shallow meridional overturning circulation. Quantifying the salt budget terms and understanding the underlying physical processes of salt transport is an important step toward understanding the oceanic water cycle. SPURS-1 research focuses on these scientific objectives in the surface salinity maximum region of the subtropical North Atlantic.

Evaporation (E) under the trade winds

exceeds precipitation (P). This maximum evaporation minus precipitation (E–P) region is located south of the salinity maximum region (SMR), resulting in an imbalance between freshwater forcing of surface salinity and surface response. Although surface water advection is known to play a role, without global salinity measurements, previous analyses have had to rely on indirect methods to estimate salinity/freshwater transport between ocean basins (e.g., Schanze et al., 2010). In considering zonal averages, advection does not completely explain the imbalance; in particular, a net imbalance between freshwater fluxes and salt advection of approximately 0.3 psu per year has been observed in the SPURS-1 latitudes (Lagerloef et al., 2010).

The Aquarius satellite provides unprecedented information on the fast, small-scale response of the ocean surface to freshwater fluxes. Questions about the spatial distribution of the imbalances and their variability can now be addressed. Here, we use surface water properties based on the latest satellite-sensed fields to revisit the salinity/freshwater balance in the North Atlantic SMR. We examine the variability and the forms of the surface forcing terms and the residual in the freshwater balance in the surface mixed layer of the SPURS-1 region, focusing on use of simple dynamics and available satellite observations to investigate the mechanisms for salt transport and exchange at the surface.

What can we learn from satellite observations about the relative roles of surface circulation and freshwater flux and their spatial and temporal structures and variability in the dynamical regions of interest? Specifically, what sets the location and boundaries of the stable high SSS region? How has the additional information on variability gained from satellite-sensed SSS changed the picture of

surface salinity evolution? Our approach is to treat the surface as a well-mixed layer and to examine observed near-surface volume transport using satellite-based surface currents.

SATELLITE OBSERVATIONS OF SALINITY AND GENERAL CIRCULATION IN THE SPURS REGION

The Ocean Surface Current Analyses Real-time (OSCAR) processing system provides surface current solutions in near-real time based on a combination of satellite-sensed sea surface height, sea surface temperature (SST), and ocean vector winds (Dohan and Maximenko, 2010). Surface currents are produced on a regular 1/3-degree grid approximately every five days by solving simplified equations of motion and averaging them over the top 30 m of the upper ocean. The geostrophic component of OSCAR includes the North Atlantic subtropical gyre, bordered along the west and north by the Gulf Stream, and eddy motions throughout the basin. The dominant wind-driven motions in OSCAR (Ekman currents) in this region are driven mostly by the trade winds.

Figure 1 plots properties averaged over the first two years of Aquarius data, collected from September 2011 to August 2013, and shows the overall features of the North Atlantic SMR: Ekman transport, geostrophic circulation, eddy activity, and freshwater flux (FWF). The 1/3-degree sea surface salinity maps are generated at Earth and Space Research using Aquarius V3.0 data. The surface current components are derived using OSCAR. OAFlux (global ocean-air fluxes; Yu et al., 2008; <http://oafux.whoi.edu>), CMORPH (a global precipitation analysis technique; Joyce et al., 2004; <http://www.cpc.ncep.noaa.gov/products/janowiak/cmorph.shtml>), and Argo float data (Roemmich

and Gilson, 2009; http://www.argo.ucsd.edu/About_Argo.html) are used for evaporation (E), precipitation (P), and mixed-layer depth (MLD ; h), respectively, to calculate the FWF term. The 37 psu contour line for the mean SSS field (Figure 1a) is

included in all plots to denote the general area of the salinity maximum and the SPURS-1 region.

Within the SPURS-1 area, $E-P$ is net positive, with a maximum located around 5° south of the SMR (Figure 1b).

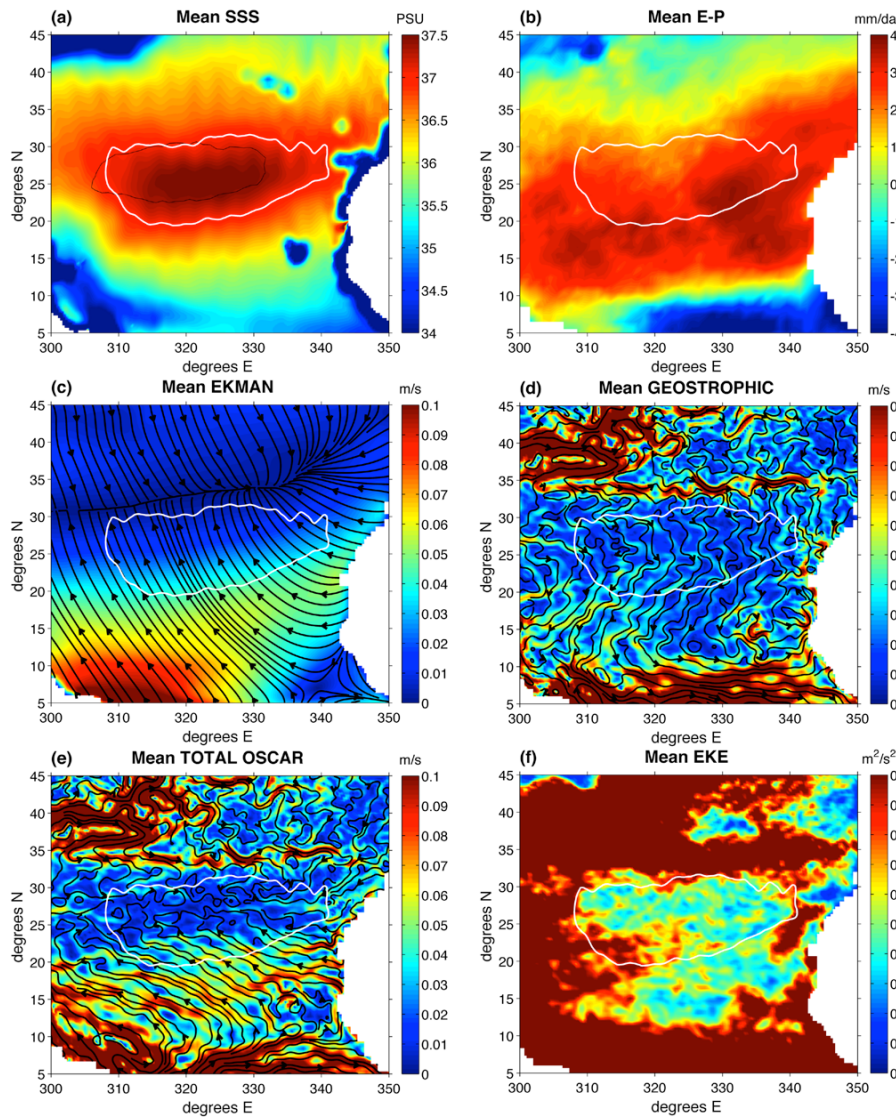


FIGURE 1. Sea surface salinity (SSS) maximum, evaporation minus precipitation ($E-P$) maximum, and general circulation in the North Atlantic, specifically, mean (a) SSS, (b) $E-P$, (c) Ekman (wind-driven) currents, (d) geostrophic currents (gyre-scale motions and eddies), (e) total surface currents from OSCAR (Ocean Surface Current Analyses Real-time), and (f) eddy kinetic energy (EKE). The time period for all data sets is from September 2011 to August 2013, the first two years of Aquarius satellite operation. The 37 psu contour (37PSUc) of mean SSS, shown in white, is included in all plots. Note the southward displacement of the net $E-P$ maximum from the SSS maximum. The Ekman currents drive northward flow. The geostrophic flow in the maximum SSS region is relatively quiet compared to the Gulf Stream and Azores currents to the north and the equatorial currents to the south. The area within the 37PSUc is comparatively void of eddies, which are a source of variability, transport, vertical motions, and mixing. The 37PSUc is within the center of the clockwise subtropical gyre, as demonstrated by the streamlines in (e). This is additionally visualized by the thin black line in (a), which marks the location where surface particles converge in this gyre. Aquarius SSS, OAFlux evaporation, CMORPH precipitation, and OSCAR current data sets were used to construct this figure.

Large-scale Ekman currents (Figure 1c) that result from the trade winds transport these salty waters northward, with a net convergence across the middle of the 37 psu contour (henceforth denoted as 37PSUc). All Figure 1 panels show the 37PSUc for the two-year time-averaged SSS plotted in white. Geostrophic currents and eddies (Figure 1d) are typically the dominant signals in most of the global ocean circulation. The 37PSUc region is a special oceanographic case in its notable lack of eddies, as indicated in the mean eddy kinetic energy (EKE) plot in Figure 1f. Here, we define eddies as the anomaly from the mean geostrophic flow. The colors are over-scaled to highlight the demarcation between eddy-rich areas north and west of the 37PSUc and the eddy-void region inside it. The northern border of the 37PSUc appears to be set by the eastward-propagating Azores current around 34°N . Although small compared to Gulf Stream eddies in the North Atlantic and equatorial currents, eddies do exist within the SMR, with maximum activity in the southwest.

The streamlines in Figure 1e show that overall subtropical gyre circulation in the 37PSUc region is clockwise and converges toward the center around 27°N . The thin black line in Figure 1a marks the convergent zone of this gyre: over 50% of particles initially placed evenly throughout the entire basin and advected by OSCAR currents over 20 years end up within this contour. This collection zone is displaced slightly northwest of the salinity maximum. The gyre circulation is composed mainly of geostrophic and Ekman currents. Southward geostrophic flow is counteracted by the northward component of a convergent meridional Ekman flow. Ekman zonal flow is westward. In considering a box around the 37PSUc, bounded by longitudes 53°W to 19°W and latitudes 19°N to 33°N and assuming constant velocities in the top 15 m, there is a mean westward surface volume transport in the top 15 m, with a total convergent zonal flow of 0.5 Sv ($1\text{ Sv} = 10^6\text{ m}^3\text{ s}^{-1}$). The meridional flow is also convergent,

TABLE 1. Mean volume transport in Sv ($10^6 \text{ m}^3 \text{ s}^{-1}$) in the top 15 m of ocean by surface currents for three regions: (1) the large salinity maximum region (SMR) containing the 37 psu contour: 53°W – 19°W , 19°N – 33°N ; (2) R-EP = the small box within the evaporation minus precipitation (E–P) max region; and (3) R-SM = the small box within the salinity maximum region. Eastward and northward flows are positive. The standard deviations of the signals in time are included.

	Through W Boundary	Through E Boundary	Through S Boundary	Through N Boundary	Net Zonal into Box	Net Meridional	Total into Box
SMR	-0.2 ± 0.4	-0.7 ± 0.4	0.8 ± 0.6	-0.6 ± 0.4	0.5	1.4	1.9 ± 0.9
R-EP	-0.3 ± 0.1	-0.3 ± 0.1	0.4 ± 0.2	0.2 ± 0.2	0.01	0.2	0.2 ± 0.2
R-SM	-0.1 ± 0.1	-0.1 ± 0.1	0.2 ± 0.2	-0.02 ± 0.2	0.04	0.2	0.3 ± 0.2

flowing into the domain from both north and south, with a total convergent surface transport of 1.4 Sv. Table 1 provides the values across each boundary. The transport values fluctuate with time on the order of the signals themselves (standard deviations are included in the table) with no clear seasonal cycle.

The picture that arises from these mean values is that Ekman currents transport salty water from the E–P max region into the 37PSUc region, a smaller portion of which is counteracted by the southward geostrophic currents, with a mean convergence into the 37PSUc. Southward flow transports freshwater from the northern boundary.

PROGRESS TOWARD FAST TIME SCALES AND SMALL SPATIAL SCALES

Prior to the launch of Aquarius/SAC-D, great success in monitoring global ocean salinity was achieved with the global array of Argo floats (Roemmich and Gilson, 2009). With over 3,000 floats spaced evenly over the ocean, one about every three degrees, measuring temperature and salinity of the upper 2,000 m, the Argo array captures the coarse seasonal cycle of the water column. Since 2011, Aquarius has been providing new insights into the smaller spatial scales and faster time scales of surface salinity.

As an illustration, Figure 2 shows a snapshot of a salinity anomaly (difference of SSS from the two-year mean) together with OSCAR geostrophic currents. Although SSS is controlled by FWF from the atmosphere as well as transport and mixing, the SSS anomalies in many

places align with velocity filaments running northwest within the instantaneous 37PSUc. Similarly, SSS anomalies are co-located with many eddies, particularly noticeable within the eddies of the Azores current at the top of the plot. The eddy activity within 37PSUc, while minor compared to neighboring areas (such as the Gulf Stream), still exhibits rich eddy activity. Eddies in the snapshot have speeds around 0.15 m s^{-1} , although stronger eddies do occasionally enter the area.

The top four panels of Figure 3 show four representative monthly plots from 2012 Aquarius SSS in the SPURS-1 region. The monthly 37PSUc is contoured in black. Aquarius gridded products perform very well when matched to Argo floats, with differences between Aquarius

SSS and Argo salinity less than 0.3 psu on average between 40°S and 40°N (Tang et al., 2014). Figure 3 demonstrates the advantage of Aquarius SSS: although the general salinity structure is captured in both the Aquarius July monthly plot (Figure 3c) and the plot made using observations from Argo (Figure 3f) for July 2012, Aquarius provides much more spatial-structure detail than Argo. Of particular note is the freshwater signal from a North Brazil Current ring forming in the bottom left corner. Island and land effects are observed as low-salinity regions along 24°W and the African continent. Aquarius calibration and validation is ongoing particularly near coasts, and while this freshwater signal is likely in part attributable to freshwater discharge from land (Tang et al., 2014), the

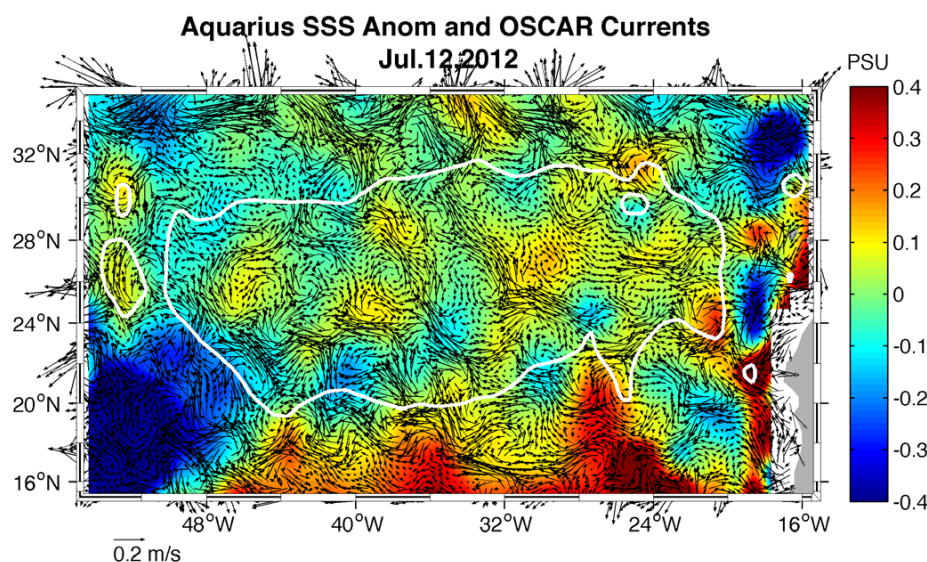


FIGURE 2. A snapshot of Aquarius SSS anomalies in color with OSCAR velocity arrows highlights the rich spatial structure available from satellite data. SSS anomalies can be seen to roughly align with filaments and eddies. The instantaneous 37 psu contour is plotted in white, showing the distortion of the edges from the mean.

degree of signal bias and distortion near land is still under investigation.

The small-scale features observable in Aquarius SSS are further highlighted in the sample salinity gradient shown in Figure 3e, which plots the absolute value of the vector salinity gradient. Salinity fronts are characterized by large salinity gradients. The SMR, previously viewed as a large area of constant surface salinity values, now shows salinity fronts throughout. These fronts are consistent across several track lines and stand out an order of magnitude above

the background gradient signal.

The relatively high resolution and regularly sampled data sets available from satellite systems allow for more focused regional studies. Two regions of interest are the salinity maximum region (R-SM) and the neighboring E-P maximum region (R-EP). Not only are they extreme cases of surface salinity, but they are also locations of convergent surface flow and the boundary of the 37PSUc. Here, we define R-SM specifically as a box in the center of the 37PSUc between 30°W and 40°W and 23°N and 28°N. The

R-EP box is defined as occurring immediately below, between 30°W and 40°W and 18°N and 23°N. The box boundaries are plotted in Figure 3a.

Looking at the local flows in around these boxes, and assuming a well-mixed layer within the top 15 m of the upper ocean, there is a net westward and northward flow in the top 15 m through R-EP, resulting in a total convergent flow of 0.2 Sv into the region due to the northward currents. In R-SM, flow is westward at about a third the magnitude of the R-EP zonal flow. Meridional currents converge with a small southward flow through the top edge for a total of 0.3 Sv convergence into the box. Table 1 provides the details. The surface volume transports tell a story of relatively strong currents outside of the 37PSUc. The northward convergent flow in the R-EP weakens with latitude and eventually reverses within the R-SM. The westward flow also weakens with latitude with a small convergence in R-SM. Eddy transport is negligible compared to the mean flows. This holds true even when considering salt transport values (not shown).

SALINITY BUDGET IN THE SURFACE MIXED LAYER

A very simple salt balance within the ocean's surface mixed layer is one in which the rate of change of salinity in time (salinity tendency) is dependent upon the freshwater surface fluxes and the advection by surface currents. Following Stevenson and Niiler (1983), the salinity tendency term ($\partial\langle S \rangle / \partial t$) is the sum of horizontal advection, FWF, and the residual terms

$$\frac{\partial\langle S \rangle}{\partial t} = -\langle \mathbf{u} \rangle \cdot \nabla \langle S \rangle + \frac{S_0(E - P)}{h} + residual \quad (1)$$

where S is mixed-layer salinity, \mathbf{u} is vector of zonal and meridional surface currents, S_0 is a representative S value, E is evaporation, P is precipitation, and angle brackets denote averaging over the MLD, h . All other processes are contained within the residual. Surface currents

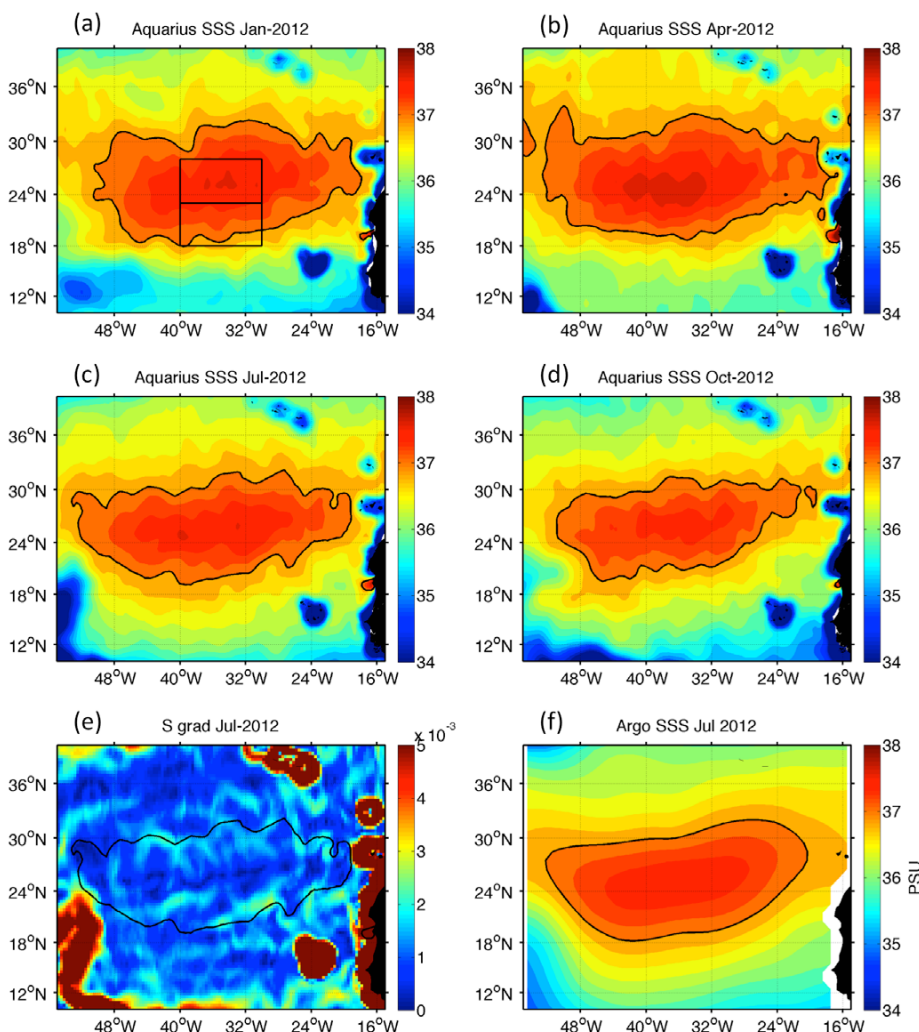


FIGURE 3. Temporal change in SSS demonstrated from sample monthly averages. The 37PSUc is plotted in black, and the contour interval is 0.2 psu. Two boxes in (a) mark regions of interest. The bottom box is the E-P max region (R-EP), and the top box is the salinity max region (R-SM). Compare the details observable in Aquarius July data (c) against the same from Argo field in (f). The finer structure in Aquarius is also evident in the magnitude of the salinity gradient field (e). Filamentary structures in SSS exist throughout. The features of the freshwater from the North Brazil Current at bottom left in (c) and (e) are also visible—features that are not observed in the corresponding Argo salinity map.

include both geostrophic and Ekman components. The form of the residual, such as the spatial distribution and the variability, therefore provides information on the potential processes that contribute to the tendency.

The residual is a nontrivial term that includes subduction, vertical shear and vertical motions, inertial waves, and all small-scale and fast dynamics, such as turbulent mixing and horizontal and vertical motions in filaments. Calculation of the terms within the residual requires velocity shear, vertical salinity and temperature gradients, and turbulence scales. The residual also includes any errors in calculations of the other terms in the equation. Discrepancies in FWF calculations between different available products can be between 0.3 psu yr^{-1} and 0.8 psu yr^{-1} in this area (Lagerloef et al., 2010). In addition, results are sensitive to the choice of the value for h . The mixed layer in this region varies seasonally between about 20 m and 125 m, with an average value of 50 m depth. Using a constant value of 30 m, for example, overestimates the FWF contribution in this area by more than 50%.

The spatial structure of each term can be seen in the two-year averaged terms in Figure 4. Aquarius SSS, although a surface measurement, is used for the mixed-layer salinity in the equation. The other terms are calculated using the satellite data sets of Figure 1. MLD from Argo is used for h . Each term is plotted on the same color scale, from -2 psu yr^{-1} to 2 psu yr^{-1} . The salinity advection term in Equation 1 is provided for full OSCAR \mathbf{u} , along with the individual geostrophic and Ekman components of OSCAR. The geostrophic component is further separated into the contribution from perturbation eddies. The FWF is mostly positive, indicating more evaporation than precipitation, with enhanced values south of the 37PSUc. The contribution to the advection term from Ekman flows is negative along the bottom half of the 37PSUc, indicating northward transport of high salinity waters. The geostrophic

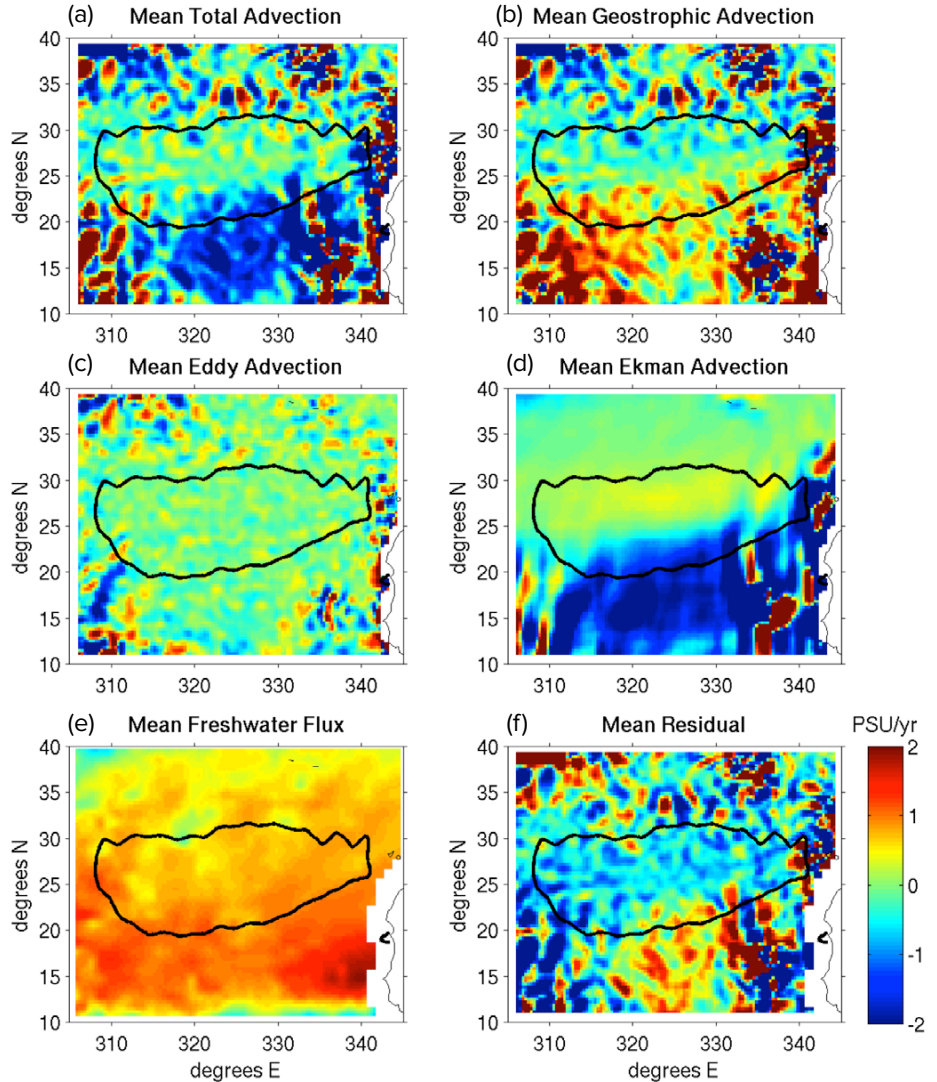


FIGURE 4. Spatial structure of the terms in the salt balance, averaged over two years. Salinity tendency = (a) Advection + (e) Freshwater Flux + (f) Residual. Advection is broken into contributions from geostrophic and Ekman components. The portion of advection by perturbation eddies within the geostrophic component is relatively very weak. The color scale is the same for all plots.

advection is opposite to the Ekman with more spatial variability. The contribution from eddies is negligible. Although eddies have zero mean speed by our definition, they may not necessarily result in a zero advection value when multiplied by the salinity gradient. The residual is on the same order as the two forcing terms, with both positive and negative areas. This is in contrast to the tendency term (not shown), which is near zero across the whole domain.

Each term in Equation 1 is variable in both space and time. To better understand this, time series of the individual terms are plotted in Figure 5. For

illustrative purposes, the eddy kinetic energy time series is included (scaled to fit). Area averages are computed within R-EP and R-SM. For clarity, monthly averages are plotted, although monthly fields obscure the daily variability in the signals. The envelopes plotted in Figure 5c are the standard deviations of the daily fluctuations of the terms within each month. For example, note that the fall of November 2012 had many rainfall events, resulting in large daily fluctuations.

Over the R-EP (Figure 5a), the FWF term (blue) tends to increase the salinity throughout the period. The sea surface salinity tendency (green) has a relatively

small temporal variation, while the horizontal advection (red) and the residual (black) terms both contribute comparable portions to balance the budget. In contrast, over the R-SM, the residual is set by the FWF because the salinity gradients are negligible in this area, resulting in a minor horizontal advection term. As a result, there is a strong seasonal cycle in the residual to balance the large seasonal FWF term.

The residual is mostly positive in the R-EP and mostly negative in the R-SM. Consistent with the mean observations in the previous section, FWF in R-EP forms saltier SSS, which is then advected northward into the R-SM. Here, the zonal flow converges, and advection cannot balance the additional FWF input. However,

when the two regions are combined (Figure 5d), FWF is mostly balanced in the temporal mean by the advection. The mean of the residual in this total region in time is $-0.09 \text{ psu yr}^{-1}$. This is in contrast to results from Argo (example plotted in Figure 5c) in which the advection term is about four-fifths the magnitude of the advection using Aquarius. This results in a larger residual and a mean imbalance of $-0.23 \text{ psu yr}^{-1}$. Both EKE and FWF show seasonal fluctuations, while the advective terms and the tendency do not. This suggests that the upper-ocean response is much slower than the atmospheric forcing.

The 37PSUc is a region of minimum variance, particularly in the residual (Figure 6). The variances in time of

the advection, FWF, and residual terms are more than two orders of magnitude lower than they are immediately outside the 37PSU region, with the exception of the very westernmost section of the 37PSUc, where there is stronger eddy activity, and along the southern border of the 37PSUc, where variability is heightened due to strong SSS gradients and variable currents.

A picture is emerging of the SMR region. The R-SM is quiet, with a low advective flux term due to smaller currents and minimal SSS gradients, low eddy activity, and low variance of forcing fields. The residual is mostly determined from the FWF. In contrast, advective terms are strong in the R-EP, and they dominate the FWF. Together, the two regions are in rough balance in the mean, although FWF has a strong seasonal cycle, while advection shows no seasonal variations.

PATHWAYS FROM THE SURFACE TO THE DEEP

Ekman pumping describes the process of upwelling/downwelling at the base of the Ekman layer due to convergences/divergences of Ekman mass transports. Figure 7a shows the vertical velocities due to Ekman pumping, calculated from wind stress curl and averaged over two years. Figure 7b shows mean vertical velocities implied by the divergence of total OSCAR currents. We used a value of 40 m depth for the Ekman layer to calculate pumping velocities from OSCAR in order to match amplitudes of Ekman velocities between OSCAR's wind-driven divergence to those obtained directly from the wind stress curl.

Regions of downwelling sweep back and forth across the 37PSUc in time, but on average, surface motions converge within the SPURS-1 region, with net downwelling within the 37PSUc. As demonstrated earlier with EKE and variance plots, the 37PSUc is at the boundary between dynamically different regions. Ekman pumping processes mostly govern the general area of downwelling,

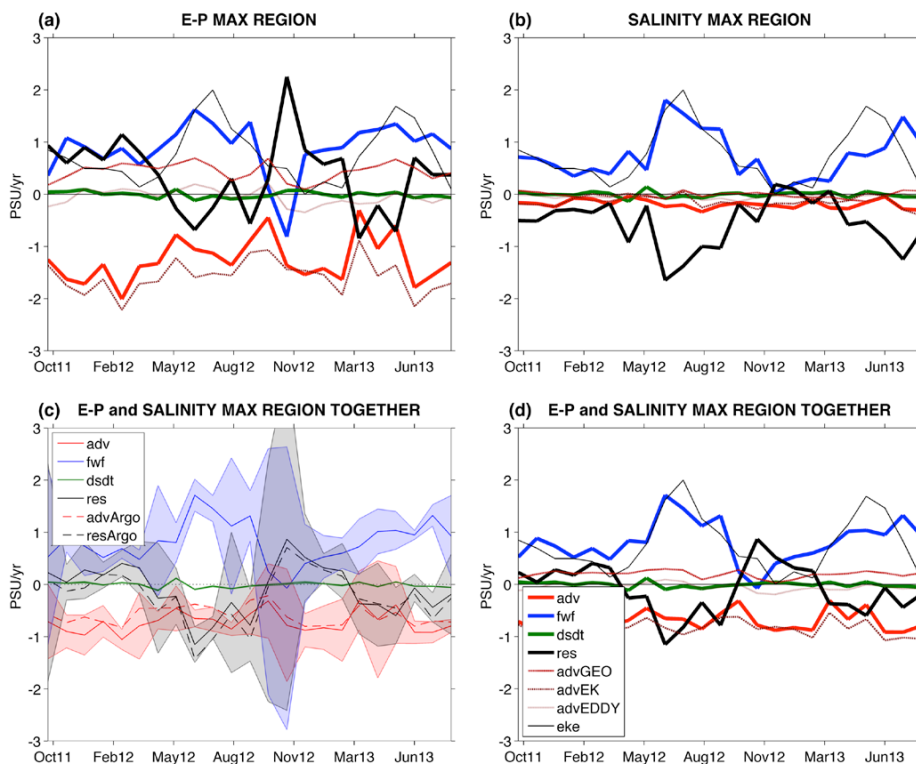


FIGURE 5. Time series of the salt budget analysis of Equation 1 in the (a) E–P maximum region and (b) salinity maximum region, and (d) combined E–P and salinity maximum region. For clarity, monthly averages are shown. Included for reference are EKE time series scaled to fit within the range of the plot. Respective contributions to the total advection term (adv) from geostrophic (advGEO) and Ekman (advEK) components of OSCAR are also included as dashed lines. The contribution to the geostrophic component from perturbation fields (advEDDY) is also shown. An example of the variability is shown in (c), which plots the same fields as (d) but with added envelopes to show temporal variability. The residual (black) shows the imbalance in each region, although when the combined effects from both regions are taken together, the residual, which shows large seasonal variability from freshwater flux, has a mean near-zero value over time. Advection terms calculated using Argo salinity in place of Aquarius are also included in (c).

although there is a slight northward shift in area for the OSCAR-based calculations, aligning the downwelling region more with the 37PSUc. The local upwelling and downwelling effects of eddies can be observed in Figure 7b.

Subduction and Deep Salt Injection

Salinity and density profiles show that salinity maximum water forming at the surface tends to subduct southwestward, governed by latitudinal temperature gradients with depth. The $\sigma_0 = 25.5$ isopycnal is a typical indicator of the North Atlantic SSS max subduction zone (Yeager and Large, 2004; Talley et al., 2011). Schmitt and Blair (2015, in this issue) describe the details of this subsurface process through analysis of the salinity maximum tongue that follows the 25.5 isopycnal in the SPURS-1 region. Observing the surface density fields based on National Oceanic and Atmospheric Administration (NOAA) Optimal Interpolation (OI) SST (Reynolds et al., 2002) and Aquarius SSS (Figure 7 bottom) as they vary with season, the 25.5 isopycnal outcrop is seen to sweep diagonally from northeast to southwest across the SMR and the 37PSUc in the wintertime. This process transports salinity to below the mixed layer and should significantly affect the residual in Equation 1. Similarly, deep winter mixed layers connect surface fluxes directly to the deep ocean.

Vertical Mixing

Salinity is also vertically transported through diapycnal mixing. Turbulence in surface mixed layers not only transports surface changes in salinity throughout the well-mixed layer, but also changes the bottom boundary, h , of our salinity budget region. Wind-forced turbulence is not the only source of mixing in the upper ocean: double diffusive convection and salt fingering also play large roles in the mixing in this area. The SMR characteristic of salty warm water lying over fresh cold water is favorable for the occurrence of double diffusion.

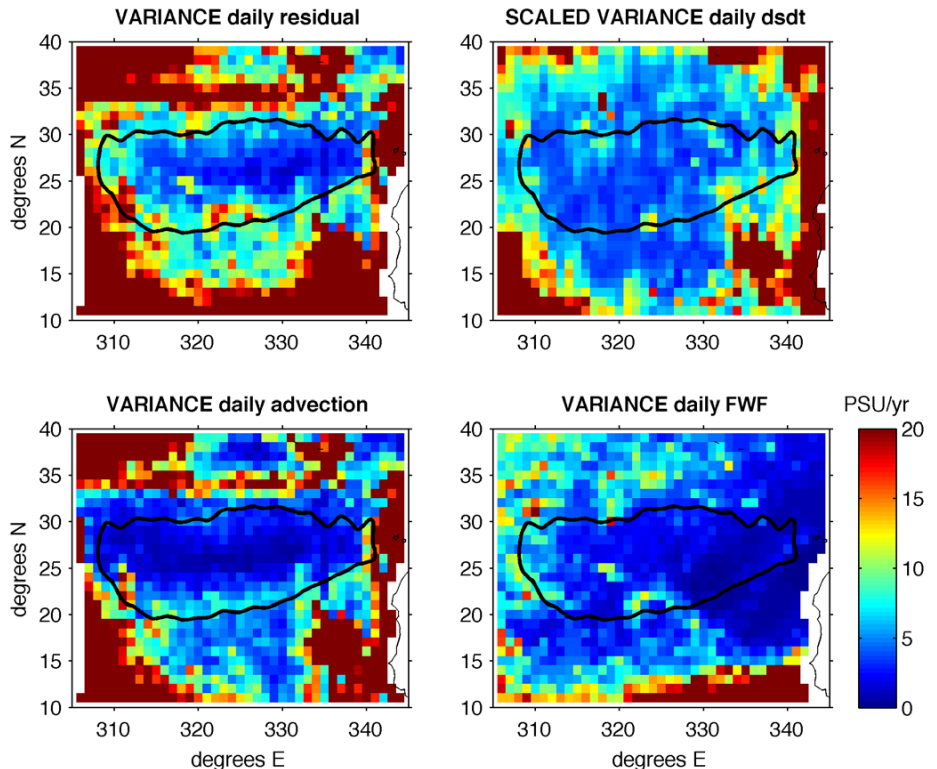


FIGURE 6. Variance of each term in the salt balance based on daily time series. The spatial distribution for each is unique, but in all there is more than an order of magnitude less variation within the 37PSUc. The ds/dt signal is so small compared to the other terms that the panel has been scaled up by 10^4 to match color scales with the others. FWF = freshwater flux.

Barrier Layers and Compensating Layers

What makes this particular area dynamically complicated is that under the E-P maximum region, salty subsurface water subducts from the north, forms a strong negative vertical salinity gradient near the surface, and results in an MLD that is shallower than the bottom of the isothermal layer. The layer of water that separates the MLD and the isothermal layer is known as a barrier layer (BL; Godfrey and Lindstrom, 1989; Lukas and Lindstrom, 1991); it appears equatorward of the subtropical gyres in every basin due to the subduction mechanism and latitudinal temperature variation (Sato et al., 2004). The existence of a BL inhibits vertical mixing of temperature and traps wind momentum in the shallow mixed layer (Maes et al., 2006). Understanding the feedback between BL thickness and air-sea interaction provides useful information for mixed-layer models and for investigation of upper-ocean processes

using surface observations.

In the SMR, salty warm surface water overlies fresh cold water beneath. The negative salinity stratification compensates the positive temperature stratification and keeps the MLD deeper than the thermocline (Yeager and Large, 2007). The region between the MLD and the isothermal layer depth is known as the compensated layer (CL; Stommel and Fedorov, 1967; de Boyer Montégut et al., 2004). Within this layer, large-scale diapycnal mixing occurs, with large vertical exchanges of temperature and salinity. Vertical advection of salt within the CL is strong, but it has not yet been quantified, and the feedback from the CL to the salinity and temperature distribution is still unknown. However, the thicknesses of the BL and the CL are key to understanding salt subduction in the SPURS regions and the indirect impact of salt on air-sea interactions. Monitoring the presence of the BL and the CL will be necessary in order to understand salinity and water mass transport.

FUTURE: CONNECTING THE TOP SURFACE TO THE MIXED LAYER AND TO THE SUBSURFACE

What processes control the sea surface salinity that Aquarius sees? Our analyses of satellite data demonstrate possible roles that the forcing terms can play in balancing the mixed-layer salt budget. Vertical processes must be subducting the SSS, as well as small-scale vertical mixing and eddy fluxes, but they cannot be captured by analysis of surface fields alone. These processes in turn rely on the dominant physics in the SMR: barrier layers, Ekman downwelling, compensating layers, turbulent diapycnal mixing, and salt injection. The frequency of observations and the spatial resolution of Aquarius, together with Argo in situ mixed-layer salinity and the extensive data set collected by the SPURS campaign, will enable us to further our understanding of the connection between the surface and the deep ocean.

SUMMARY

New features in the surface salinity signal have been observed in Aquarius SSS. Satellite systems can provide frequent, regular sampling that results in high spatial resolution surface data and enables better understanding of the processes that contribute to the freshwater cycle. The 37PSUc in the middle of the North Atlantic subtropical gyre marks the divide between several dynamical processes. It indicates the region of maximum SSS, very small SSS tendency, very low eddy activity, convergent surface flow throughout, and very low variance in the surface forcing terms for SSS. This SMR lies north of the maximum evaporation region. Although there is a seasonal cycle to the imbalance of the simple freshwater flux equation, and two-year means show a residual that is spatially variable, regional studies reveal areas in which the freshwater input,

together with the advection by surface currents, can yield a net year-mean balance. Freshwater flux terms have strong seasonal cycles, while advection terms do not. However, the story is not one of a simple one-dimensional vertical surface exchange. The constant SMR is maintained by northward Ekman flow, countered by southward geostrophic flow, with potentially very strong contributions from the vertical processes of subduction and deep mixed-layer injection. These processes, which connect the surface to the deep, are further complicated by barrier layers and compensating layers below the surface. Much remains to be learned by continued study of the connection between the surface and the deep utilizing the advantages of satellite data to provide regular frequent sampling of the surface exchange, together with the intensive in situ observations gathered below the surface during SPURS. ©

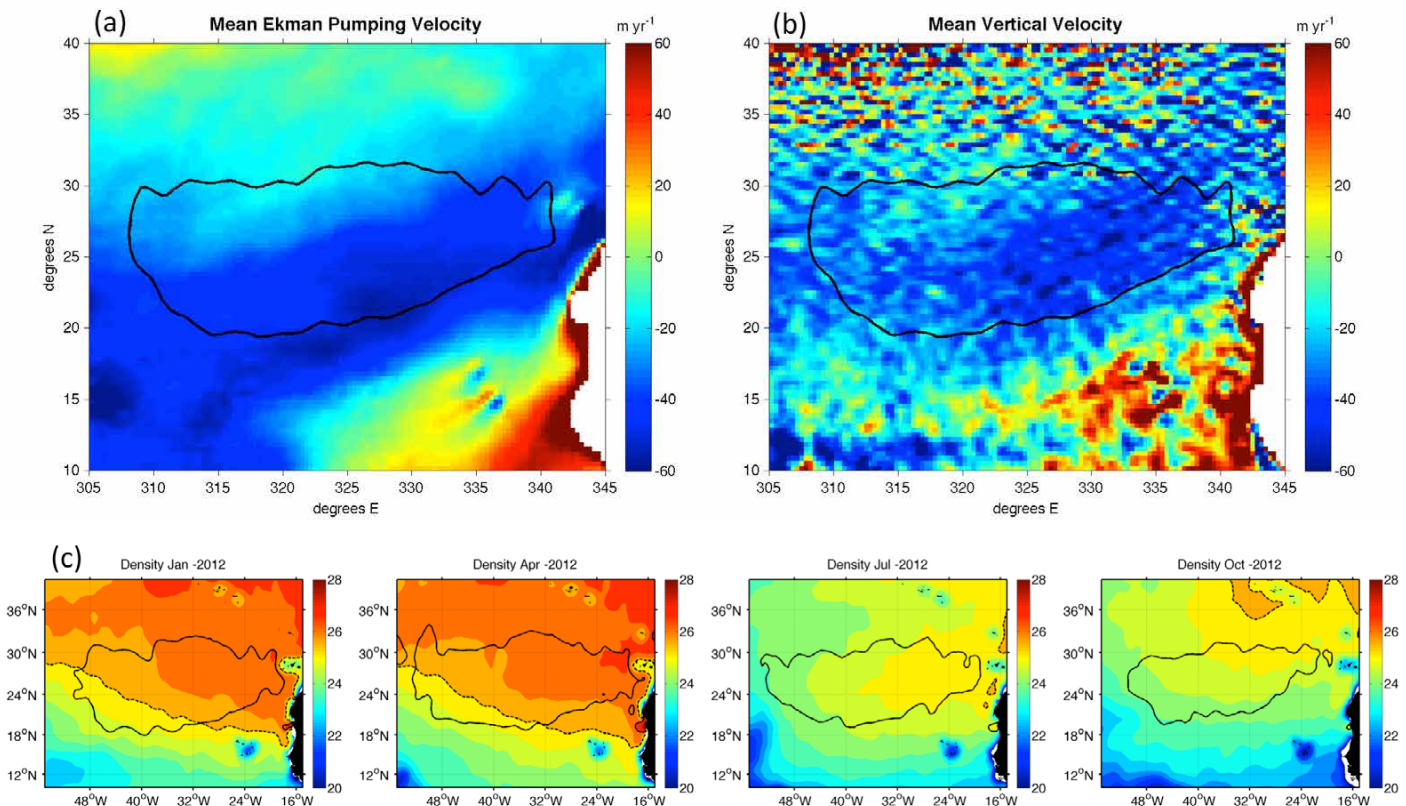


FIGURE 7. Connecting vertical processes with the surface. (a) Vertical velocities at the base of the mixed layer induced by Ekman pumping calculated from wind stress curl. (b) Vertical velocities induced by total surface horizontal convergences. Negative values indicate areas of downwelling throughout the entire salinity maximum region (SMR). (c) Seasonal cycle of density σ_0 at the surface in difference from $1,000 \text{ kg m}^{-3}$. The $\sigma_0 = 25.5$ contour (dashed line) is a known indicator of subduction zones and isopycnal outcroppings. Contour interval is 0.5 kg m^{-3} . This outcropping sweeps across the SMR during the winter and is a likely contributor to the salinity imbalance.

REFERENCES

- de Boyer Montégut, C., G. Madec, A.S. Fisher, A. Lazar, and D. Iudicone. 2004. Mixed layer depth over the global ocean: An examination of profile data and a profile-based climatology. *Journal of Geophysical Research* 109, C12003, <http://dx.doi.org/10.1029/2004JC002378>.
- Dohan, K., and N. Maximenko. 2010. Monitoring ocean currents with satellite sensors. *Oceanography* 23(4):94–103, <http://dx.doi.org/10.5670/oceanog.2010.08>.
- Godfrey, J.S., and E.J. Lindstrom. 1989. The heat budget of the equatorial western Pacific surface mixed layer. *Journal of Geophysical Research* 94:8,007–8,017, <http://dx.doi.org/10.1029/JC094iC06p08007>.
- Joyce, R.J., J.E. Janowiak, P.A. Arkin, and P. Xie. 2004. CMORPH: A method that produces global precipitation estimates from passive microwave and infrared data at high spatial and temporal resolution. *Journal of Hydrometeorology* 5:487–503, [http://dx.doi.org/10.1175/1525-7541\(2004\)005<0487:CAMTPG>2.0.CO;2](http://dx.doi.org/10.1175/1525-7541(2004)005<0487:CAMTPG>2.0.CO;2).
- Lagerloef, G. 2014. Sea surface salinity. Pp. 747–754 in *Encyclopedia of Remote Sensing*. E.G. Njoku, ed., Springer, New York, http://dx.doi.org/10.1007/978-0-387-36699-9_165.
- Lagerloef, G., R. Schmitt, J. Schanze, and H.-Y. Kao. 2010. The ocean and the global water cycle. *Oceanography* 23(4):82–93, <http://dx.doi.org/10.5670/oceanog.2010.07>.
- Lagerloef, G., F. Wentz, S. Yeuh, H.-Y. Kao, G. Johnson, and J. Lyman. 2012. Aquarius satellite mission provides new detailed view of sea surface salinity. In State of the Climate in 2011, *Bulletin of the American Meteorological Society* 93(7):S70–S71.
- Lukas, R., and E. Lindstrom. 1991. The mixed layer of the western equatorial Pacific Ocean. *Journal of Geophysical Research* 96(S01):3,343–3,357, <http://dx.doi.org/10.1029/90JC01951>.
- Maes, C., K. Ando, T. Delcroix, W.S. Kessler, M.J. McPhaden, and D. Roemmich. 2006. Observed correlation of surface salinity, temperature and barrier layer at the eastern edge of the western Pacific warm pool. *Geophysical Research Letters* 33, L06,601, <http://dx.doi.org/10.1029/2005GL024772>.
- Reynolds, R.W., N.A. Rayner, T.M. Smith, D.C. Stokes, and W. Wang. 2002. An improved in situ and satellite SST analysis for climate. *Journal of Climate* 15:1,609–1,625, [http://dx.doi.org/10.1175/1520-0442\(2002\)015<1609:AIISAS>2.0.CO;2](http://dx.doi.org/10.1175/1520-0442(2002)015<1609:AIISAS>2.0.CO;2).
- Roemmich, D., and J. Gilson. 2009. The 2004–2008 mean and annual cycle of temperature, salinity, and steric height in the global ocean from the Argo Program. *Progress in Oceanography* 82:81–100, <http://dx.doi.org/10.1016/j.pocean.2009.03.004>.
- Sato, K., T. Suga, and K. Hanawa. 2004. Barrier layer in the North Pacific subtropical gyre. *Geophysical Research Letters* 31, L05,301, <http://dx.doi.org/10.1029/2003GL018590>.
- Schanze, J., R. Schmitt, and L. Yu. 2010. The global oceanic freshwater cycle: A state-of-the-art quantification. *Journal of Marine Research* 68:569–595, <http://dx.doi.org/10.1357/002224010794657164>.
- Schmitt, R.W., and A. Blair. 2015. A river of salt. *Oceanography* 28(1):40–45, <http://dx.doi.org/10.5670/oceanog.2015.04>.
- Stevenson, J.W., and P.P. Niiler. 1983. Upper ocean heat budget during the Hawaii-to-Tahiti shuttle experiment. *Journal of Physical Oceanography* 13:1,894–1,907, [http://dx.doi.org/10.1175/1520-0485\(1983\)013<1894:UOHBDT>2.0.CO;2](http://dx.doi.org/10.1175/1520-0485(1983)013<1894:UOHBDT>2.0.CO;2).
- Stommel, H., and K.N. Fedorov. 1967. Small scale structure in temperature and salinity near Timor and Mindanao. *Tellus* 19:306–325, <http://dx.doi.org/10.1111/j.2153-3490.1967.tb01484.x>.
- Talley, L.D., G.L. Pickard, W.J. Emery, and J.H. Swift. 2011. Section 9.8.2.2 in *Descriptive Physical Oceanography: An Introduction*, sixth ed. Elsevier Science, Boston.
- Tang, W., S.H. Yueh, A.G. Fore, and A. Hayashi. 2014. Validation of Aquarius sea surface salinity with in situ measurements from Argo floats and moored buoys. *Journal of Geophysical Research* 119:6,171–6,189, <http://dx.doi.org/10.1002/2014JC010101>.
- Yeager, S.G., and W.G. Large. 2004. Late-winter generation of spiciness on subducted isopycnals. *Journal of Physical Oceanography* 34:1,528–1,547, [http://dx.doi.org/10.1175/1520-0485\(2004\)034<1528:LGOSOS>2.0.CO;2](http://dx.doi.org/10.1175/1520-0485(2004)034<1528:LGOSOS>2.0.CO;2).
- Yeager, S.G., and W.G. Large. 2007. Observational evidence of winter spice injection. *Journal of Physical Oceanography* 37:2,895–2,919, <http://dx.doi.org/10.1175/2007JPO36291>.
- Yu, L., X. Jin, and R. Weller. 2008. Multidecade global flux datasets from the objectively analyzed air-sea fluxes (OAFux) project: Latent and sensible heat fluxes, ocean evaporation, and related surface meteorological variables. OAFux Project Technical Report (OA-2008-01), Woods Hole Oceanographic Institution.

AUTHORS. **Kathleen Dohan** (kdohan@esr.org) is Senior Scientist and Principal Investigator for the OSCAR project, Earth and Space Research, Seattle, WA, USA. **Hsun-Ying Kao** is Research Scientist, Earth and Space Research, Seattle, WA, USA. **Gary S.E. Lagerloef** is Senior Scientist and Principal Investigator, NASA Aquarius Mission, Earth and Space Research, Seattle, WA, USA.

ARTICLE CITATION

Dohan, K., H.-Y. Kao, and G.S.E. Lagerloef. 2015. The freshwater balance over the North Atlantic SPURS domain from Aquarius satellite salinity, OSCAR satellite surface currents, and some simplified approaches. *Oceanography* 28(1):86–95, <http://dx.doi.org/10.5670/oceanog.2015.07>.